Monthly Notices
of the
ROYAL ASTRONOMICAL SOCIETY

MNRAS **505,** 5833–5845 (2021)
Advance Access publication 2021 June 17

https://doi.org/10.1093/mnras/stab1720

Does jackknife scale really matter for accurate large-scale structure covariances?

Ginevra Favole [1]★ Benjamin R. Granett [2] Javier Silva Lafaurie[3] and Domenico Sapone[3]

[1] *Institute of Physics, Laboratory of Astrophysics, Ecole Polytechnique Fédérale de Lausanne (EPFL), Observatoire de Sauverny, CH-1290 Versoix, Switzerland*
[2] *INAF-Osservatorio Astronomico di Brera, via Brera 28, 20121 Milano, and via E. Bianchi 46, I-23807, Merate, Italy*
[3] *Grupo de Cosmología y Astrofísica Teórica, Departamento de Física, FCFM, Universidad de Chile, Blanco Encalada 2008, Santiago, Chile*

Accepted 2021 June 13. Received 2021 June 8; in original form 2021 April 28

ABSTRACT

The jackknife method gives an internal covariance estimate for large-scale structure surveys and allows model-independent errors on cosmological parameters. Using the SDSS-III BOSS CMASS sample, we study how the jackknife size and number of resamplings impact the precision of the covariance estimate on the correlation function multipoles and the error on the inferred baryon acoustic scale. We compare the measurement with the MultiDark Patchy mock galaxy catalogues, and we also validate it against a set of lognormal mocks with the same survey geometry. We build several jackknife configurations that vary in size and number of resamplings. We introduce the Hartlap factor in the covariance estimate that depends on the number of jackknife resamplings. We also find that it is useful to apply the tapering scheme to estimate the precision matrix from a limited number of resamplings. The results from CMASS and mock catalogues show that the error estimate of the baryon acoustic scale does not depend on the jackknife scale. For the shift parameter α, we find an average error of 1.6 per cent, 2.2 per cent and 1.2 per cent, respectively, from CMASS, Patchy, and lognormal jackknife covariances. Despite these uncertainties fluctuate significantly due to some structural limitations of the jackknife method, our α estimates are in reasonable agreement with published pre-reconstruction analyses. Jackknife methods will provide valuable and complementary covariance estimates for future large-scale structure surveys.

Key words: galaxies: haloes – galaxies: statistics – cosmological parameters – large-scale structure of Universe – cosmology: observations – cosmology: theory .

1 INTRODUCTION

The most popular methods to estimate the uncertainties on the galaxy two-point correlation function (2PCF) internally in a survey are bootstrap (Efron 1979; Davison & Hinkley 1997; Norberg et al. 2009, 2011) and jackknife (Quenouille 1956; Miller 1974; Turkey 1958; Norberg et al. 2009, 2011) resampling. Bootstrap resampling is carried out by randomly selecting N_b sub-volumes, with replacement, from the original sample. Then the galaxy clustering measurement is performed in each resampling, which is associated a constant weight equal to the number of times that the sub-volume has been selected (Norberg et al. 2009). Similarly, the jackknife method uses N_{jk} regions in the survey footprint, each with approximately the same volume. The correlation function is measured on the survey multiple times, each time removing a different jackknife region (Norberg et al. 2009). The covariance matrix is finally inferred from the 2PCF measurements and the 1σ errors are derived as the square root of the diagonal elements.

Internal methods for error estimation are computationally inexpensive and are derived directly from the measurements. Therefore, the analysis does not depend on an assumed cosmological model, which is an attractive feature when testing alternative models such as dark energy or modified gravity. Indeed, jackknife resampling has been widely used to estimate the uncertainties on the galaxy clustering measurements from large-volume spectroscopic surveys (see e.g. Zehavi et al. 2002, 2005, 2011; Anderson et al. 2012; Guo et al. 2013; Ross et al. 2012; Guo et al. 2015a, b; Favole et al. 2016a, 2017).

Jackknife resampling has two main disadvantages: (i) it tends to overestimate the errors due to the lack of independence between the N_{JK} copies and (ii) it is necessary to balance the number and size of resamplings to be drawn in the survey footprint. The last issue is driven by several factors. First of all, in order to have covariances with reduced noise in their off-diagonal terms, we need a large number of jackknife resamplings. This limits the size of the jackknife regions and also the maximum scales that can be probed in the galaxy clustering observables. It is often assumed in the literature that the jackknife cell size S_{JK} should embed the maximum scale measured in the two-point correlation functions. At the same time, to have an invertible (i.e. non-singular) covariance matrix, the number of resamplings should be larger than the number of bins in the measured 2PCF. These conditions are difficult to satisfy in galaxy samples with limited area (e.g. Beutler et al. 2011; Hong, Han & Wen 2016). Due to the finite size of any survey footprint, the more resamplings we draw, the smaller their size and the variation between one copy and the next one (Norberg et al. 2009, 2011).

★ E-mail: ginevra.favole@epfl.ch

The issues discussed above have discouraged some cosmologists to use jackknife resampling in favour of estimating the galaxy clustering uncertainties from large sets of independent synthetic galaxy catalogues. In the last years, the advent of efficient codes based on fast gravity solvers has considerably reduced the computational time needed for massive mock production, making available many different realizations of accurate, independent mocks for covariance estimates. Among these methods, PTHALOS (Scoccimarro & Sheth 2002; Manera et al. 2013), PINOCCHIO (Monaco, Theuns & Taffoni 2002; Monaco et al. 2013), PATCHY (Kitaura et al. 2016), and HALOGEN (Avila et al. 2015) are all based on Lagrangian perturbation theory (LPT). Others, such as QPM (White, Tinker & McBride 2014), FastPM (Feng et al. 2016), or PPM-GLAM (Klypin & Prada 2018), use a quick particle mesh approach. Algorithms such as EZ-MOCKS (Chuang et al. 2015a) adopt the effective Zel'dovich approximation, while COLA (Tassev, Zaldarriaga & Eisenstein 2013; Koda et al. 2016), L-PICOLA (Howlett, Manera & Percival 2015), or ICE-COLA (Izard, Crocce & Fosalba 2016) combine LPT with *N*-body solvers to speed up the computational time. Finally, high-fidelity mocks can also be obtained from multiple realizations of a lognormal density field (Coles & Jones 1991; Beutler et al. 2011; Hong et al. 2016; Agrawal et al. 2017; Lippich et al. 2019), or populating dark matter haloes with galaxies using the halo occupation distribution technique (HOD; e.g. Berlind & Weinberg 2002; Zheng et al. 2005).

All these fast mocking approaches are extremely convenient compared to running a full *N*-body code, but they are generally limited to predicting the dark matter distribution. On top of the dark matter field, it is necessary to model the galaxy distribution by properly accounting for the different baryonic components and the complex physics of galaxy formation and evolution (e.g. Mo, van den Bosch & White 2010; Naab & Ostriker 2017).

Simulating baryons is a non-trivial task, which requires advanced computational techniques and resources. Semi-analytic models of galaxy formation and evolution (SAMs; White & Frenk 1991; Kauffmann, White & Guiderdoni 1993; Baugh 2006; Cora 2006; Croton et al. 2006, 2016; Benson 2010, 2012; Gargiulo et al. 2015; Somerville & Davé 2015; Collacchioni et al. 2018; Cora et al. 2018) and hydrodynamical simulations (e.g. Yepes et al. 1997; Springel & Hernquist 2003; Yoshida et al. 2003; Springel 2010; Vogelsberger et al. 2014b, a; Genel et al. 2014; Crain et al. 2015; Schaye et al. 2015; Pillepich et al. 2018) are now able, with different degrees of accuracy, to incorporate the multitude of ingredients and physical processes that contribute to shape the formation and evolution of galaxies within their host dark matter haloes. Some of these processes are gas accretion (Guo et al. 2011; Henriques et al. 2013; Hirschmann, De Lucia & Fontanot 2016) and cooling (De Lucia et al. 2010; Monaco et al. 2014; Hou, Lacey & Frenk 2018), star formation (Lagos et al. 2011), stellar winds (Lagos, Lacey & Baugh 2013), stellar evolution (Tonini et al. 2009; Henriques et al. 2011; Gonzalez-Perez et al. 2014), AGN feedback (Bower et al. 2006; Croton et al. 2006), or environmental processes (Weinmann et al. 2006; Font et al. 2008; Stevens & Brown 2017; Collacchioni et al. 2018).

Analogously, one should also account for the effect of massive neutrinos on the growth of cold dark matter perturbations, which are responsible of suppressing the matter power spectrum at intermediate and small scales (Ali-Haïmoud & Bird 2013; Wright, Winther & Koyama 2017; Parimbelli, Viel & Sefusatti 2019).

All of these assumptions and prescriptions have uncertainties which become significant on non-linear scales and limit the accuracy of the covariance estimate.

Upcoming surveys, such as the Dark Energy Spectroscopic Instrument[1] (DESI; Schlegel et al. 2015), Euclid[2] (Laureijs et al. 2011; Sartoris et al. 2016) and the Large Synoptic Survey Telescope[3] (LSST; Ivezić et al. 2019), will bring us to the era of high-precision cosmology. In order to prepare to this new phase, it is imperative to improve and compare different methods to construct accurate covariances able to capture the hidden physical process of gravitational collapse. These methods have to carefully optimize the specific binning scheme adopted in order to minimize the noise in the measurements.

For the reasons above, in this work we aim to rehabilitate the use of jackknife resamplings versus mocks for estimating covariances. We explore how varying the size ($S_{\rm JK}$) and number ($N_{\rm JK}$) of jackknife regions impacts the precision in the error estimates of galaxy clustering and on the baryon acoustic oscillation scale through the α shift parameter. In concrete, we measure the monopole and quadrupole two-point correlation functions of the BOSS CMASS DR12 galaxies and we compute their covariances using four different jackknife configurations, coupled with two binning schemes. We compare these results with those obtained from 1000 MultiDark Patchy mocks implemented for BOSS DR12 (Kitaura et al. 2016) and with the average covariance obtained by performing jackknife resampling on 10 Patchy mocks, randomly chosen among the 1000. We then contrast these results with 1000 independent lognormal mocks with the same volume of CMASS, and we also perform the jackknife analysis on 10 of the lognormal mock realizations.

From these covariances, we build the precision matrices needed to estimate the α shift parameter through a Monte Carlo Markov Chain (MCMC) algorithm. We reduce the noise in their off-diagonal terms by applying the tapering correction (Kaufman, Schervish & Nychka 2008). We study the impact of a variation in the tapering parameter, $T_{\rm p}$, on the α results. These estimates of α will be directly compared with the galaxy clustering pre-reconstruction results from the BOSS collaboration (Ross et al. 2016).

The paper is organized as follows. In Section 2, we introduce the observational galaxy sample used in our analysis, SDSS-III/BOSS CMASS DR12. In Section 3, we present the galaxy clustering measurements performed, together with the jackknife methodology and schemes used to estimate their uncertainties. Section 4 describes the models adopted to analyse the CMASS observations: the MultiDark Patchy mocks (Section 4.1), the lognormal ones (Section 4.2), and the analytic models constructed for the Monte Carlo runs (Section 4.3). In Section 5, we explain the Monte Carlo algorithm used to extract the α BAO parameter. Section 6 presents our main results, which are discussed in Section 7, together with our conclusions.

Throughout the paper, we adopt a Planck et al. (2014) cosmology with $\Omega_{\rm m} = 0.307115$, $\Omega_\Lambda = 0.692885$, $h = 0.6777$, $n = 0.9611$, and $\sigma_8 = 0.8228$.

2 OBSERVED GALAXY SAMPLE: BOSS CMASS DR12

The SDSS-III BOSS survey observed about 1.2 million galaxies over an effective area of 9329 deg^2 (Alam et al. 2017), using the 2.5m Sloan Telescope (Gunn et al. 2006) at the Apache Point Observatory in New Mexico. It used a drift-scanning mosaic CCD camera with

[1] https://www.desi.lbl.gov
[2] https://www.euclid-ec.org
[3] https://www.lsst.org

five photometric bands, *ugriz* (Gunn et al. 1998; Fukugita et al. 1996), and two spectrographs covering the wavelength range of 3600–10000Å with a resolving power of 1500 to 2600 (Smee et al. 2013). Spectroscopic redshifts were measured using the minimum-χ^2 template-fitting procedure by Aihara et al. (2011), with templates from Bolton et al. (2012).

BOSS targeted galaxies into two main samples: LOWZ at $z < 0.43$ and CMASS at $0.43 < z < 0.7$ (Ahn et al. 2012). For our analysis, we use the data from the BOSS CMASS DR12 sample (Alam et al. 2015; Reid et al. 2016; Alam et al. 2017), which is defined through a number of magnitude and colour cuts aimed at obtaining a selection of galaxies with approximately constant stellar mass (see e.g. Reid et al. 2016).

3 MEASUREMENTS

3.1 Two-point correlation functions

We measure the two-point correlation function, $\xi(s, \mu)$, of the galaxy sample described in Section 2 using the code from Favole et al. (2017). This is based on the Landy–Szalay estimator (Landy & Szalay 1993),

$$\xi(s, \mu) = \frac{DD(s, \mu) - 2DR(s, \mu) + RR(s, \mu)}{RR(s, \mu)}, \quad (1)$$

where s is the redshift-space distance and μ is the cosine of the angle between s and the line of sight.

In the expression above, *DD*, *DR*, and *RR* are, respectively, the data–data, data–random, and random–random pair counts that we can form between the galaxy and random catalogues. The latter is built to have the same angular footprint and radial distribution of the CMASS observations. All the pairs above are properly normalized by the number of galaxies (randoms) and weighted to correct from different systematic effects (see e.g. Sánchez et al. 2012; Ross et al. 2012; Favole et al. 2016b). In particular, we weight the observed data for potential fibre collisions ($w_{\rm fc}$) and for redshift failures ($w_{\rm zf}$). We also account for possible variation in the galaxy (random) number densities assuming the FKP (Feldman, Kaiser & Peacock 1994) weight:

$$w_{\rm FKP} = \frac{1}{1 + n(z)P_0}, \quad (2)$$

where $n(z)$ is the galaxy (random) number density at redshift z and P_0 is a constant quantity that roughly corresponds to the amplitude of the CMASS power spectrum at $k = 0.1\,h{\rm Mpc}^{-1}$. We assume $P_0 = 20000\,h^3{\rm Mpc}^{-3}$ as in Anderson et al. (2012).

From equation (1), we compute the multipoles of the CMASS correlation function as

$$\xi_l(s) = \frac{2l+1}{2} \int_{-1}^{1} \xi(s, \mu) P_l(\mu)\, {\rm d}\mu, \quad (3)$$

where $P_l(\mu)$ are the Legendre polynomials. In this study, we focus only on the first two even multipoles of the 2PCF, i.e. the monopole $\xi_0(s)$ and the quadrupole $\xi_2(s)$. We explore two different binning schemes, both centred on the BAO distance scale, coupled with the jackknife configurations defined in Section 3.2: (i) 20 linear bins in $24 < s < 184\,h^{-1}$Mpc and 120 linear bins in $0 < \mu < 1$; (ii) 10 linear bins in $24 < s < 184\,h^{-1}$Mpc and 120 linear bins in $0 < \mu < 1$.

Table 1. Jackknife configurations adopted in our analysis. For each of the four cases implemented, we indicate the number of jackknife resamplings ($N_{\rm JK}$), the area ($A_{\rm JK}$) and comoving size ($S_{\rm JK}$) of the individual cell computed in Planck et al. (2014) cosmology at the mean redshift of CMASS, $z = 0.56$.

$N_{\rm JK}$	$A_{\rm JK}$ (deg^2)	$S_{\rm JK}$ (h^{-1}Mpc)
200	46.6	110.7
100	93.3	156.6
50	186.6	221.4
20	932.9	495.1

3.2 Jackknife configurations and covariances

We implement jackknife resampling in the BOSS CMASS DR12 galaxy sample following a standard prescription (see e.g. Norberg et al. 2009, 2011) and adopting four different configurations, which are summarized in Table 1. We divide the survey footprint into 200, 100, 50, and 20 RA × DEC cells approximately containing the same number of galaxies (randoms). Since the bias changes with redshift, we choose not to vary the size of the jackknife regions in the line-of-sight direction, as they would not be representative of the clustering signal. The CMASS covariance matrix for $N_{\rm JK}$ jackknife resamplings is (e.g. Ross et al. 2012; Favole et al. 2016a):

$$C_{\rm ij} = \frac{N_{\rm JK} - 1}{N_{\rm JK}} \sum_{\rm a=1}^{N_{\rm JK}} (\xi_{\rm i}^a - \bar{\xi}_{\rm i})(\xi_{\rm j}^a - \bar{\xi}_{\rm j}), \quad (4)$$

where $\bar{\xi}_i$ is the mean jackknife correlation function in the ith bin,

$$\bar{\xi}_{\rm i} = \sum_{\rm a=1}^{N_{\rm JK}} \xi_{\rm i}^a / N_{\rm JK}. \quad (5)$$

The overall factor in equation (4) corrects from the lack of independence between the $N_{\rm JK}$ jackknife copies, which is the main limitation of the jackknife method. In fact, from one configuration to the next, $N_{\rm JK} - 2$ cells are the same (Norberg et al. 2011).

4 MODELS

4.1 MultiDark Patchy mock galaxy catalogues

In order to analyse the CMASS two-point correlation function multipoles, we use 1000 MultiDark Patchy mocks implemented for BOSS DR12 (Kitaura et al. 2016; Rodríguez-Torres et al. 2016). These were constructed using the Patchy code (Kitaura, Yepes & Prada 2014), which couples second-order Lagrangian perturbation theory (2LPT; see e.g. Buchert 1994; Bouchet et al. 1995; Catelan et al. 1995) with a spherical collapse model (Bernardeau 1994; Mohayaee et al. 2006; Neyrinck 2013) to generate a dark matter field on a mesh (Kitaura & Hess 2013). The mesh has been populated with galaxies using a deterministic and a stochastic bias, whose parameters were constrained to precisely match the two- and three-point statistics (Kitaura et al. 2015).

The Patchy mocks were built assuming the same ΛCDM Planck cosmology adopted in this work (see Section 1), and they were calibrated against N-body-based reference catalogues through sub-halo abundance matching to recover the survey geometry, selection function, galaxy number density and clustering bias of BOSS data

in 10 redshift bins (Rodríguez-Torres et al. 2016). Previous studies (e.g. Chuang et al. 2015b; Kitaura et al. 2016; Rodríguez-Torres et al. 2016) have demonstrated that the Patchy mocks are very accurate in reproducing the two- and three-point statistics of BOSS data.

4.2 Lognormal mock galaxy catalogues

Besides the Patchy mocks described in the previous section, we perform the analysis also using a set of 1000 lognormal mock galaxy catalogues that we generate for the BOSS CMASS sample at mean redshift $z \sim 0.56$. In this way, we validate the accuracy of our lognormal mock algorithm, which is a useful tool for future studies, with a much lower computational cost compared to the Patchy method.

The target power spectrum for our LN mocks was computed with the code *CLASS*[4] (Blas, Lesgourgues & Tram 2011), assuming the formalism used for our analytic models and given in equation (10). We have then applied a linear bias and the Halofit (Takahashi et al. 2012) prescription to model the non-linear galaxy power spectrum: $P_{\rm nl}(k) = b^2 P(k) + ck^{-3}$ with the value $b = 1.87$ and $c = 0.021$. The k^{-3} term is used to match the amplitude of the correlation function on BAO scales and is motivated by the similar nuisance parameters introduced in the BAO fitting procedure (equation 13). The free parameters in the model were tuned to match the measured CMASS monopole correlation function.

We present the *Synmock* code used to produce the lognormal catalogues in a public repository.[5] The implementation follows the standard approach for generating lognormal simulations (see also Beutler et al. 2011; Pearson, Samushia & Gagrani 2016). For each realization, first we generated a Gaussian density field $\delta_G(\vec{x})$ on a cubic grid with dimension $L = 4096h^{-1}$Mpc and step size $h = 4h^{-1}$Mpc and transformed it to derive the target lognormal field:

$$\delta(\vec{x}) = \exp\left(\delta_G(\vec{x}) - \sigma^2/2\right) - 1, \tag{6}$$

where σ^2 is the variance of the Gaussian field. In order to match the target power spectrum, we made a Fourier transform of the power spectrum to compute the correlation function and using the relationship (Coles & Jones 1991)

$$\xi_G(|\vec{x} - \vec{x}'|) = \log\left(1 + \xi(|\vec{x} - \vec{x}'|)\right). \tag{7}$$

The lognormal density field was used to build a discrete galaxy field by Poisson sampling the number density $n(\vec{x}) = \bar{n}(1 + \delta(\vec{x}))$. We applied a uniform random offset to move the mock galaxies away from the grid points.

The velocity field was computed on the same $\delta(x)$ grid using the linear continuity equation in Fourier space:

$$\vec{v}\left(\vec{k}\right) = i\frac{faH}{b}\delta\left(\vec{k}\right)\frac{\vec{k}}{k^2}, \tag{8}$$

where f is the logarithmic growth rate. After a final Fourier transform, the velocity of each galaxy was assigned using the value at the nearest grid point.

We built 1000 BOSS CMASS realizations ('LN mocks', hereafter) with $0.43 < z < 0.7$ by cutting the BOSS survey geometry in the lognormal simulation box above. The Cartesian galaxy coordinates were transformed to the spherical coordinates right ascension, declination, and radial distance with the origin at the centre of the simulation box. In order to transform to the redshift-space coordinates, the line-of-sight peculiar velocity component was computed and applied to the radial comoving distance: $r_s = r + \vec{r}\cdot\vec{v}/(aH|\vec{r}|)$. We constructed a coarse angular mask using the Healpix (Górski et al. 2005) scheme at resolution $n_{\rm side} = 64$ and discarded galaxies outside the mask. The catalogue was further downsampled along the radial direction to match the target redshift distribution. We generated an unclustered random catalogue with 10 times the number density of the CMASS data that precisely corresponds to the mock construction using the same angular mask and radial selection function.

After computing the correlation functions of the $N_{\rm LN} = 1000$ lognormal mocks, we derive their covariance matrix as

$$C_{\rm ij} = \frac{1}{N_{\rm LN} - 1}\sum_{\rm a=1}^{N_{\rm LN}}(\xi_{\rm i}^a - \bar{\xi}_{\rm i})(\xi_{\rm j}^a - \bar{\xi}_{\rm j}), \tag{9}$$

where $\bar{\xi}_{\rm i}$ is their mean 2PCF in the ith bin. The pre-factor properly accounts for the fact that the mock realizations are independent.

4.3 Analytic models

Besides the Patchy and the LN mocks, we also model the multipoles of the BOSS CMASS two-point correlation function using an analytic approach, which is required to run the Monte Carlo analysis (see Section 5). The 2PCF can be obtained from the Fourier transform of the matter power spectrum, $P(k)$, for which we assume the template from Padmanabhan & White (2008):

$$P(k) = [P_{\rm lin}(k) - P_{\rm dw}(k)]\, e^{-k^2\Sigma_{\rm nl}^2/2} + P_{\rm dw}(k). \tag{10}$$

In the equation above, $P_{\rm lin}(k)$ is the linear matter power spectrum computed using the Boltzmann code CLASS (Lesgourgues 2011), assuming the Planck 2015 (Ade et al. 2016) fiducial cosmology. The $P_{dw}(k)$ term is the de-wiggled power spectrum (Eisenstein & Hu 1998), while the Σ_{nl} parameter encodes the smoothing of the BAO peak due to non-linear effects (Crocce & Scoccimarro 2006). The multipoles of the analytic 2PCF are defined as

$$\xi_l(s) = \frac{i^l}{2\pi^2}\int_0^\infty P_l(k)\, j_l(ks)k^2{\rm d}k, \tag{11}$$

from which we recover the monopole ($l = 0$) and the quadrupole ($l = 2$). In equation (11), $j_l(x)$ represents the spherical Bessel function of first kind and order l, while $P_l(k)$ are the multipoles of the power spectrum defined as

$$P_l(k) = \frac{2l+1}{2}\int_{-1}^{1}\left(1 + f\mu^2\right)^2 P(k)L_l(\mu){\rm d}\mu, \tag{12}$$

where $L_l(x)$ is the Legendre polynomial of order l and $P(k)$ is the template given in equation (10). By replacing equation (12) in equation (11), the analytic expressions for monopole ($l = 0$) and quadrupole ($l = 2$) are respectively (Xu et al. 2012):

$$\xi^{(0)}_{\rm model}(s) = B_0\xi_0(\alpha s) + a_0^{(0)} + \frac{a_1^{(0)}}{s} + \frac{a_2^{(0)}}{s^2}, \tag{13}$$

$$\xi^{(2)}_{\rm model}(s) = B_2\xi_2(\alpha s) + a_0^{(2)} + \frac{a_1^{(2)}}{s} + \frac{a_2^{(2)}}{s^2}, \tag{14}$$

where α is the shift parameter, while $(a_1^{(i)}, a_2^{(i)}, a_3^{(i)})$ are linear nuisance parameters.

The shift parameter α in equations (13) and (14) is usually defined as (Padmanabhan & White 2008)

$$\alpha = \frac{D_V}{r_s}\frac{r_s^{\rm fid}}{D_V^{\rm fid}}, \tag{15}$$

[4] https://github.com/lesgourg/class_public
[5] https://github.com/bengranett/synmock

where r_s represents the sound horizon (Hu & Sugiyama 1996), and D_V the volume-averaged distance given by (Eisenstein et al. 2005)

$$D_{\rm V}(z) = \left[cz(1+z)^2 D_{\rm A}^2(z) H^{-1}(z)\right]^{1/3}, \tag{16}$$

with $D_{\rm A}(z)$ being the angular diameter distance, and $H(z)$ the Hubble parameter at redshift z. The α shift parameter accounts for the observed distortion between distances due to the chosen fiducial cosmology, while the nuisance parameters $(a_1^{(i)}, a_2^{(i)}, a_3^{(i)})$ and B_1, B_2 incorporate those effects that are responsible of modulating the clustering amplitude, such as redshift-space distortions (Xu et al. 2012), linear bias, and the power spectrum normalization, σ_8.

5 SHIFT PARAMETER ESTIMATION

Following the methodology presented in Favole, Sapone & Silva Lafaurie (2019), we analyse the BOSS CMASS covariances from jackknife, and the Patchy and LN ones with and without jackknife, using a Monte Carlo Markov Chain based on a Metropolis–Hastings algorithm.[6] Our MCMC code is publicly available on GitHub.[7]

In order to find the optimal parameter values, we assume a likelihood function $\mathcal{L} \propto \exp(-\chi^2/2)$, with

$$\chi^2 = \left(\vec{\xi}_{\rm model} - \vec{\xi}_{\rm obs}\right)^T \hat{\Psi} \left(\vec{\xi}_{\rm model} - \vec{\xi}_{\rm obs}\right), \tag{17}$$

where

$$\vec{\xi}_{\rm model} \equiv \left(\vec{\xi}^{(0)}_{\rm model}, \vec{\xi}^{(2)}_{\rm model}\right) \tag{18}$$

represents the theoretical correlation function whose components are given in equations (13)–(14), while $\vec{\xi}_{\rm obs}$ corresponds to the observed CMASS 2PCF, with its monopole and quadrupole moments grouped in a vector as a function of the comoving distance:

$$\vec{\xi}_{\rm obs} \equiv \left(\vec{\xi}^{(0)}_{\rm CMASS}, \vec{\xi}^{(2)}_{\rm CMASS}\right). \tag{19}$$

The Ψ term in equation (17) is the precision matrix defined as

$$\hat{\Psi} = \left(1 - \frac{n_{\rm b}+1}{N_{\rm res}-1}\right) \left(\hat{C} \circ T\right)^{-1} \circ T, \tag{20}$$

where $\hat{C}$ is the total assembled covariance matrix from the individual auto- and cross-covariances either obtained from 1000 mock realizations of from jackknife resamplings:

$$\hat{C} = \begin{pmatrix} \hat{C}_{\xi_0\xi_0} & \hat{C}_{\xi_0\xi_2} \\ \hat{C}^T_{\xi_0\xi_2} & \hat{C}_{\xi_2\xi_2} \end{pmatrix}. \tag{21}$$

The first term in parenthesis in equation (20) is the Hartlap correction factor (Hartlap, Simon & Schneider 2007), which corrects from the bias introduced in the covariance matrix by the limited number of jackknife resamplings and 2PCF bins. In Table 2, we report the values of the Hartlap factor as a function of the number of jackknife resamplings and bins used in our analysis. In the last row of the table, we also show the value of the Hartlap correction for 20 spatial bins and 1000 mock realizations, i.e. our ideal 1000 Patchy/LN configurations. In these cases the Hartlap correction is almost negligible, as it is very close to unity. The lower the number of bins and jackknife resamplings, the stronger the effect of such a correction.

The quantity T in equation (20) is the tapering correction (Kaufman et al. 2008) that minimizes the noise in the off-diagonal terms of the covariance matrix; for further details, see also Favole et al. (2019). In this work, we assume a tapering parameter $T_{\rm p} = 500\,{\rm h^{-1}Mpc}$ to ensure that the entire covariance matrix is positive semidefinite and the deviations in the off-diagonal terms are minimized. In Section 6, we test how a variation in the tapering parameter affects the results for α and its uncertainty. Further details on the dependence of α on $T_{\rm p}$ are addressed also in Paz & Sánchez (2015).

Table 2. Values of the Hartlap factor (Hartlap et al. 2007) as a function of the number of bins $n_{\rm b}$ and jackknife resamplings $N_{\rm JK}$ used in our analysis. In the last row, we also show the value of the Hartlap correction for our ideal 1000 Patchy/LN mocks.

$n_{\rm b}$	$N_{\rm JK}$	Hartlap correction
10	20	0.42105
20	50	0.57143
20	100	0.78788
20	200	0.89447
20	1000	0.97898

6 RESULTS

In Fig. 1, we present the BOSS CMASS monopole and quadrupole two-point autocorrelation functions compared to the mean predictions from the 1000 Patchy and LN mocks, and the analytic model defined in Section 4.3. The CMASS error bars are inferred from the jackknife covariances based on the four configurations shown in Table 1 coupled with two different binning schemes (see Section 3.1). For the Patchy and LN mocks, we show the dispersion obtained from their 1000 realizations without applying any jackknife resampling. The LN mocks reproduce the BAO peak well, while the Patchy result differ from the CMASS measurements in the broadband shape. The LN monopole prediction tends to overestimate the observed clustering amplitude at $s \lesssim 60\,h^{-1}$Mpc and beyond $150\,h^{-1}$Mpc. Patchy, instead, reproduces well the CMASS clustering up to $\sim 80\,h^{-1}$Mpc and underestimates it beyond BAO scales. The systematic difference in shape will be accounted for by the nuisance parameters in the model and so it will not influence the analysis of the α shift parameter. We also overplot the analytic 2PCF model used in our MCMC algorithm to extract the α BAO parameter (see Section 5). The best-fitting analytic model is in good agreement with the CMASS multipole measurements on all scales.

In Fig. 2, we compare the normalized monopole and quadrupole covariances from the 1000 Patchy (upper triangle) and the 1000 LN (lower triangle) mocks. These measurements are both built in 20 s bins, without applying any jackknife resampling. The matrix is normalized as $C_{ij}^{\rm norm} = C_{ij}/\sqrt{C_{ii}\,C_{jj}}$, with C_{ij} given in equation (9). Despite the number of Patchy and LN mocks used here is the same, the LN result shows a higher covariance in the off-diagonal terms. The LN mocks are based on a number of approximations that prevent them from capturing the full non-linear effects, which instead are included in the Patchy mocks (see also Blot et al. 2019).

In the left column of Fig. 3, we compare the average normalized covariances obtained by performing jackknife resamplings on 10 different LN realizations (upper triangles) versus BOSS CMASS data (lower triangles). In the right column are the average covariances of 10 different Patchy mocks (upper triangles) and CMASS data (lower). In each column, from top to bottom, we show the 20, 50,

[6] https://emcee.readthedocs.io/en/stable/
[7] https://github.com/javiersilvalafaurie/BTCosmo

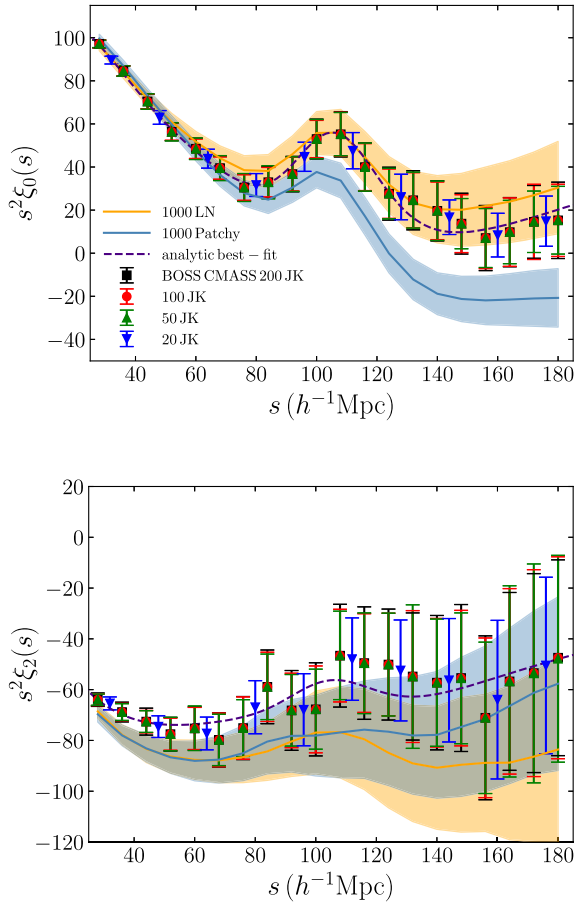

Figure 1. Monopole (top) and quadrupole (bottom) autocorrelation functions of the BOSS CMASS galaxies (markers) computed, using two different binning schemes (20 and 10 linear bins in s) coupled with the jackknife configurations given in Table 1 for the error estimation (200, 100, 50, 20 resamplings). We overplot in turquoise (orange) the mean $\pm\sigma$ values from the 1000 Patchy (LN) mocks. The analytic best-fitting models to the CMASS measurements that we use to estimate the α shift parameter (see Section 4.3) are shown as dashed purple curves.

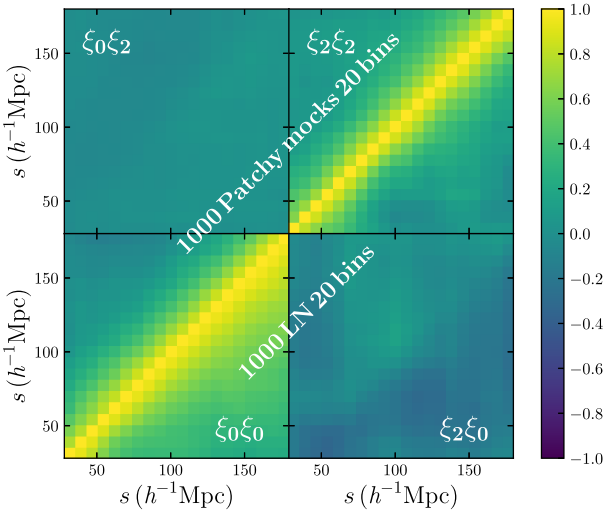

Figure 2. Normalized monopole and quadrupole auto- and cross-covariances obtained from the 1000 Patchy (upper triangle) versus the 1000 LN (lower triangle) mocks, without applying any jackknife resampling. The normalization is computed as $C_{\rm ij}^{\rm norm} = C_{\rm ij}/\sqrt{C_{\rm ii}\,C_{\rm jj}}$, where $C_{\rm ij}$ is given in equation (9). The mean value and $1\,\sigma$ dispersion of these mocks are shown in Fig. 1 as solid lines with the corresponding shaded region.

100, and 200 jackknife configurations listed in Table 1, respectively, coupled with 10, 20, 20, 20 linear bins in s (see Section 3). The normalization is calculated as described in Fig. 2, with $C_{\rm ij}$ given by equation (4). It is evident that the noise in the covariance estimates is reduced as the number of resamplings is increased. The covariances in 20 bins obtained from 200 jackknife resamplings on the Patchy, LN mocks or CMASS observations are consistent with the results from 1000 Patchy and LN mocks without jackknife shown in Fig. 2. These covariances lead to consistent error bars on the galaxy clustering multipoles, as we can appreciate in Fig. 1.

In Fig. 4, we compare the average normalized jackknife covariances from LN and Patchy mocks versus their reference covariances from 1000 independent realizations already shown in Fig. 2. There is a systematic difference in the covariances. The noise in the off-diagonal terms of the JK covariances is larger compared to the reference covariances and reduces as the number of jackknife regions increases.

Fig. 5 shows, as a function of the scale, the ratios of the jackknife variances and the 1000 independent Patchy or LN mocks. In the top panels are the results from CMASS jackknife against the reference mocks. The bottom panels show the average uncertainties from jackknife on 10 Patchy/LN realizations against the 1000 reference mocks without jackknife.

We remind the reader that the 200, 100, and 50 JK configurations are measured in 20 s bins, while the 20 JK case in 10 bins. The combined action of the jackknife size, number and binning is what determines the level of noise in the covariances. In Fig. 5, we see that the 20 JK scheme always leads to the largest fluctuations in the σ estimate due to having relatively few jackknife resamplings available. However, doing only 10 bins instead of 20 helps to partially mitigate these fluctuations.

On small scales, the errors from CMASS jackknife shown in the top panels of Fig. 5 are underestimated with respect to the 1000 reference Patchy or LN mocks by up to ~ 40 per cent, for both monopole and quadrupole. This effect is mitigated when the number of jackknife resamplings increases.

Beyond BAO scales, we observe the opposite trend, with CMASS jackknife errors tendentially overestimated with respect to the ideal cases. Around $130\,h^{-1}$Mpc, the monopole errors from CMASS covariances are $\sim$ 10–50 per cent larger than those from 1000 Patchy or LN mocks and the discrepancy overall increases with the number of resamplings. Compared to the monopole, the quadrupole shows smaller fluctuations in the 1σ ratio shown in the top panels of Fig. 5.

The amplitude of the quadrupole 20 JK result is $\sim$ 10–20 per cent lower than the others on scales below $150\,h^{-1}$Mpc; the monopole is lower than the rest on about all scales when compared to the 1000 Patchy mocks, and only beyond $140\,h^{-1}$Mpc when compared to the 1000 LN. As expected, the 20 and 50 jackknife schemes return the largest fluctuations. Although larger jackknife regions with greater independence may give a more accurate covariance estimate, the uncertainty on the covariance is large due to having few resamplings available. In the 20 JK scheme coupled with 10 s bins, the large fluctuations produced by a limited number of resamplings are partially mitigated by the smaller number of bins compared to the other cases.

In the bottom panels of Fig. 5, we display the ratios of the average variance from jackknife resamplings on 10 Patchy or LN realizations and that from the 1000 independent mocks of reference. The Patchy

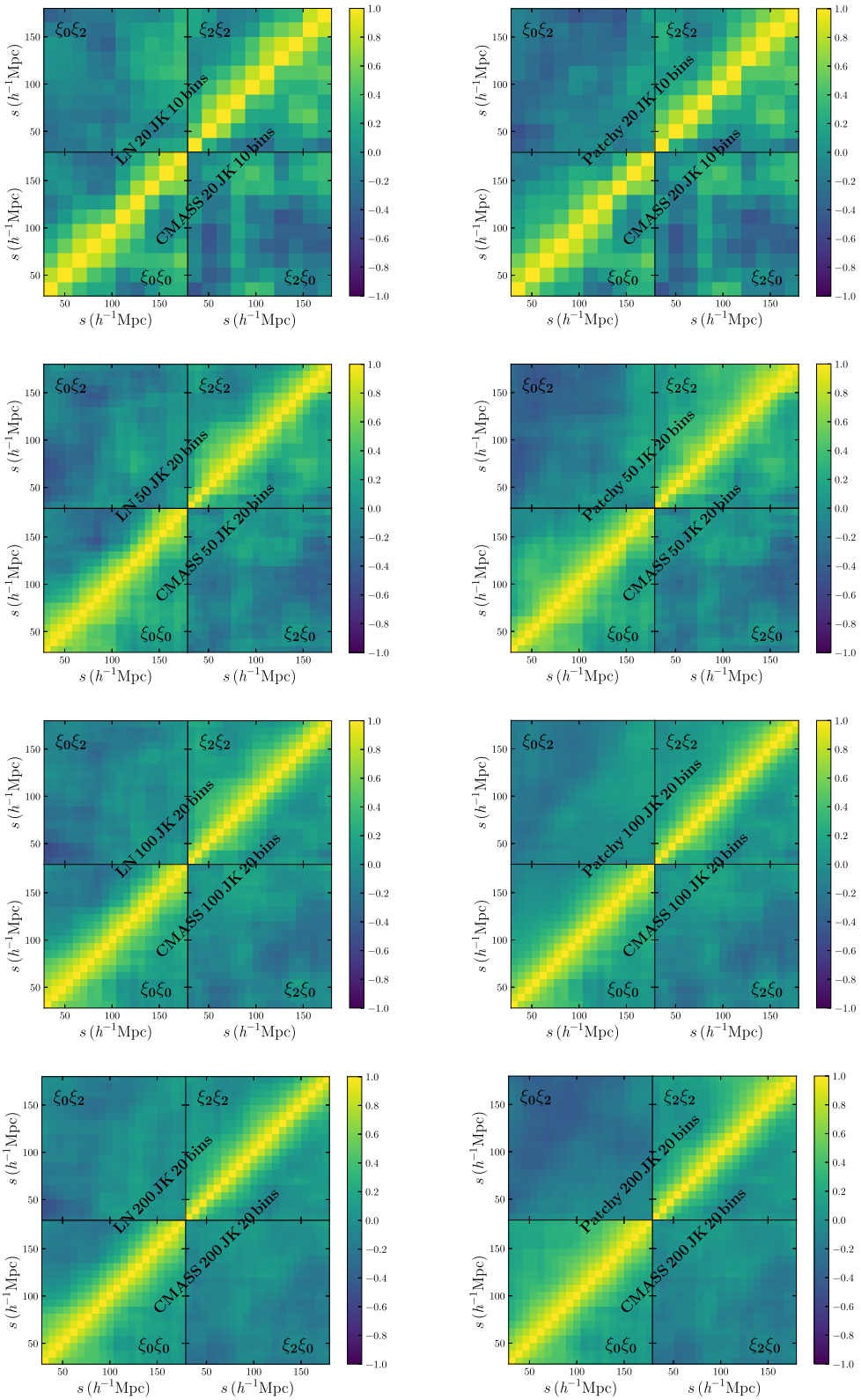

Figure 3. Normalized covariances obtained from jackknife resampling performed on 10 different LN and Patchy realizations (upper triangles) and on BOSS CMASS data (lower triangles). For both the LN and Patchy results, we show the average estimate from the 10 covariances. From top to bottom, we display the 20, 50, 100, and 200 jackknife configurations coupled with two binning schemes.

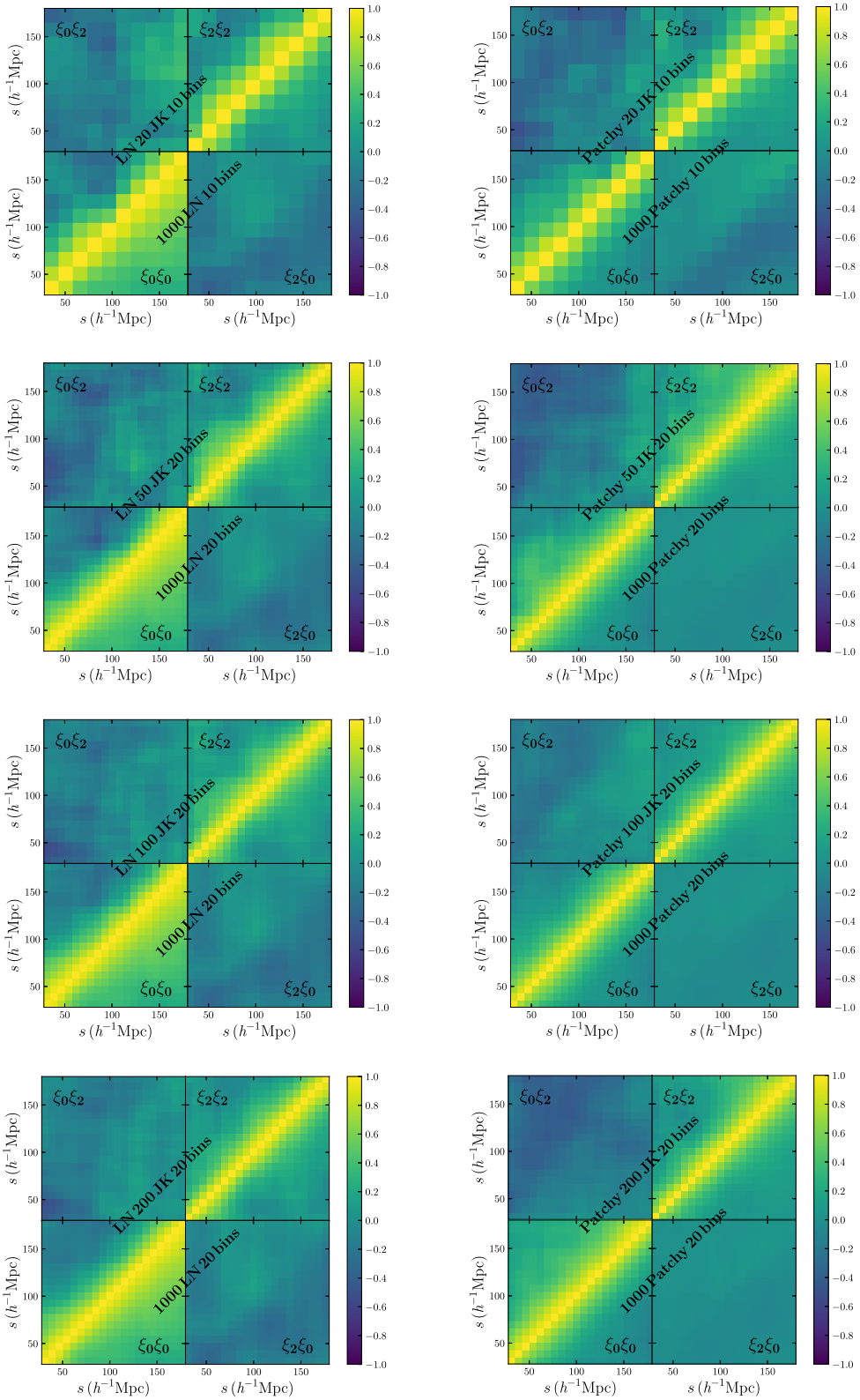

Figure 4. Same result as Fig. 3, but here in the lower triangles we show the reference covariances from 1000 LN and Patchy mocks without jackknife, which are also shown in Fig. 2. Normalized covariances obtained from jackknife resampling performed on 10 different LN and Patchy realizations (upper triangles) and on BOSS CMASS data (lower triangles). In the upper triangles, we show the average estimate from the covariances of 10 mock realizations.

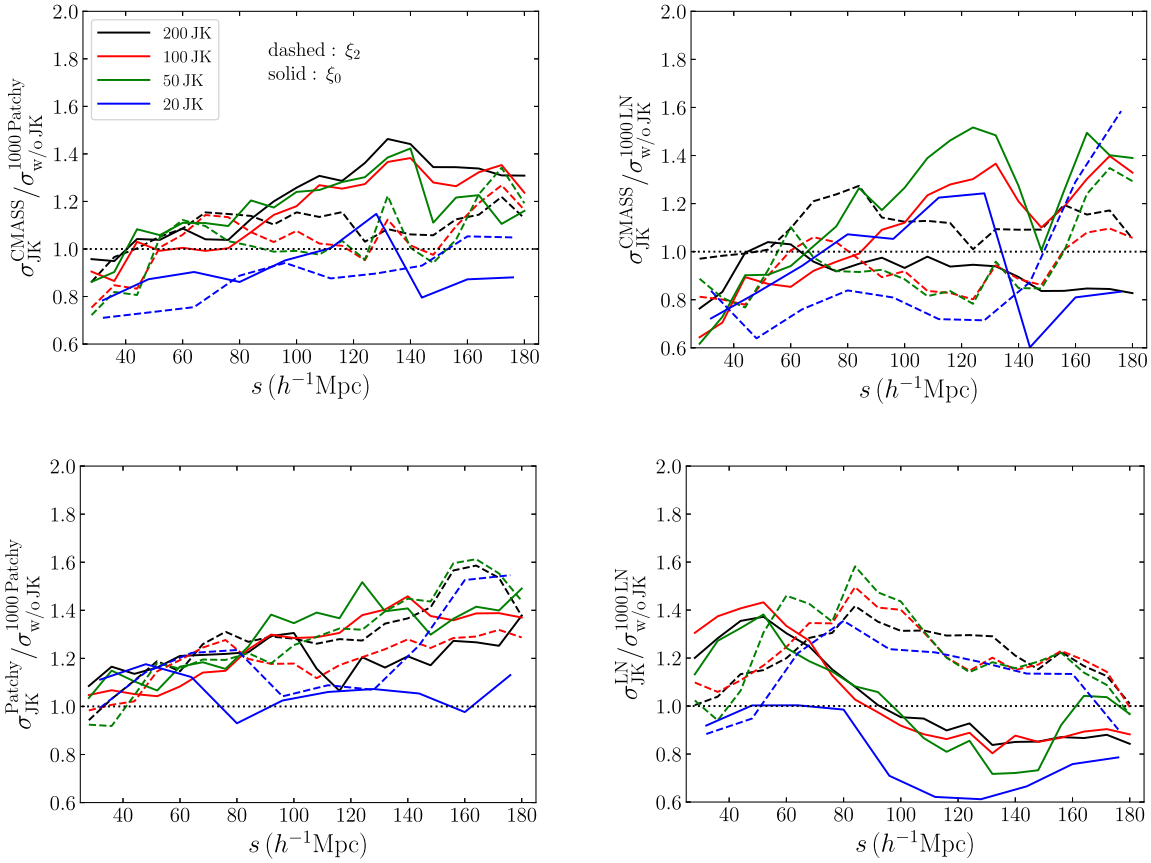

Figure 5. Top row: Ratios between the 1σ uncertainties obtained from the CMASS jackknife covariances and the 1000 Patchy (left) or LN (right) mocks without JK. The solid (dashed) lines correspond to the monopole (quadrupole) measurements. Bottom row: Ratios between the average $1\,\sigma$ errors obtained from jackknife resamplings on 10 different Patchy (left) and the LN (right) realizations and those from 1000 Patchy or LN without jackknife. We remind the reader that the 200, 100, and 50 JK configurations are coupled with 20 s bins, while the 20 JK case with 10 bins. The monopole and quadrupole results are shown as solid and dashed lines, respectively. The horizontal dotted lines are shown to help the comparison.

JK outcomes show similar fluctuations and trends to the CMASS results shown in the top left-hand panel, with deviations from the reference uncertainties of up to 40–50 per cent on large scales.

On the other hand, the LN jackknife ratios exhibit flatter trends, similar to the CMASS results in the top right-hand panel. The biggest difference is seen in the LN JK monopole signals, which are overestimated (underestimated) on small (large) scales by up to $\sim$ 50 per cent ($\sim$ 40 per cent). Beyond $\sim 150\,h^{-1}$Mpc, the monopole (quadrupole) errors from LN jackknife seems to converge to the results from 1000 LN independent mocks. Again, the 20 and 50 JK configurations are the ones exhibiting the largest fluctuations due to the limited number of jackknife resamplings.

Overall, we find reasonable agreement between the uncertainties from jackknife on CMASS, Patchy or LN mocks with the same volume of CMASS, and from 1000 independent Patchy/LN realizations. In general, with respect to the 1000 reference mocks representing the ideal case, the monopole errors from CMASS JK are underestimated on small scales and overestimated beyond $\sim 80\,h^{-1}$Mpc, those from Patchy JK are overestimated on all scales, and those from LN JK are overestimated below $\sim 80\,h^{-1}$Mpc and underestimated beyond. For the quadrupole, the CMASS JK errors are overestimated (underestimated) compared to the 1000 Patchy (LN) mocks of reference, while those from Patchy (LN) jackknife are overestimated compared to both 1000 Patchy and LN mocks. All these discrepancies remain within 30 per cent in most cases.

Despite the use of only 10 mock realization is not sufficient to clearly identify general trends, the jackknife variances in Fig. 5 reveal deviations from that of the full set of mocks. For Patchy, these differences increase on larger scales in both multipoles, while for the LN mocks they peak on smaller and intermediate scales. These deviations are due to the known limitations of the jackknife method which, nevertheless, provides covariance estimates in reasonable agreement with those from multiple mock realizations.

We next analyse the impact of the different covariance estimates on the error of the α shift parameter. Fig. 6 compares the α values and corresponding uncertainties obtained from the covariances based on (i) BOSS CMASS JK, (ii) Patchy/LN JK, and (iii) 1000 independent Patchy/LN mocks. For each jackknife configuration performed on the LN or Patchy mocks, we show the average α value from 10 different realizations randomly chosen. In general, a sample size of 10 is sufficient to infer the mean and scatter with a precision of $\sim$30 per cent. Compared with just a single mock, in this way we improve the precision of the error estimate by $\sqrt{10}$. These results are reported in Table 3 and assume a tapering parameter $T_{\rm p} = 500$, which we found to be optimal.

Overall, we find good agreement between the results based on covariances from jackknife, both applied to CMASS observations, LN and Patchy mocks. The 1000 LN and Patchy results without jackknife are consistent with the JK outcomes, despite the difference in the pre-factor of their covariances (equations 4 and 9) and

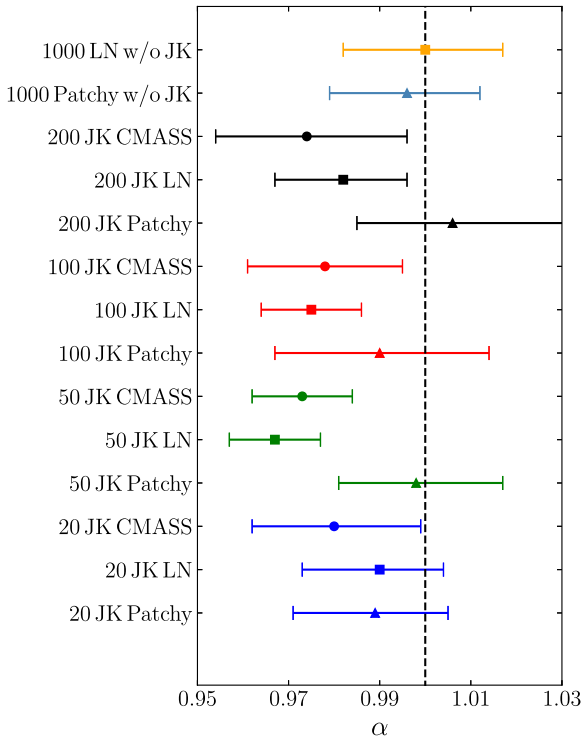

Figure 6. Summary of the α shift parameters obtained from the covariances calculated either using the 1000 independent mock realizations, or the JK configurations and binning schemes reported in Table 3. The results from JK on LN or Patchy are the average values of 10 α estimates, each one obtained from a different mock realization. The points are colour-coded as in Fig. 1, where each colour corresponds to a different jackknife/binning scheme. The results from CMASS are represented by dots, those from LN by squares and those for Patchy mocks by triangles. The vertical line shows the value $\alpha = 1$ to help the comparison. All these results are calculated, assuming a tapering parameter $T_{\rm p} = 500$.

the difference in the structure of their off-diagonal terms (see Fig. 2).

The uncertainties on α are all in agreement with each other, independently from the number/size of jackknife resamplings adopted. The average errors obtained from 200, 100, and 50 JK resamplings (i.e. the most robust ones) performed on CMASS data, 10 LN and 10 Patchy mocks are ~ 1.6 per cent, ~ 1.2 per cent, and 2.2 per cent, respectively. Those from the 1000 LN and Patchy covariances without jackknife are ~ 1.7 per cent and ~ 1.6 per cent, respectively. These last two cases are ideal since the 1000 LN and Patchy mocks are all independent (but we do not expect the lognormal mocks to capture the full covariance of the CMASS galaxy sample). The 50 and 20 JK schemes are the ones returning the largest fluctuations in the covariances, which can result in errors on α as large as ~ 1.9 per cent. These are not the largest uncertainties on α, which instead come from the 200 JK and 100 JK Patchy configurations. In order to quantify the fluctuations, we have repeated all the jackknife resamplings on 10 different realizations of both the LN and Patchy mocks.

The constraints on α presented in Fig. 6 do not show a clear trend with $N_{\rm JK}$, and highlight a different behaviour between the Patchy and the LN mocks, which seems to converge for the 20 JK case.

In Fig. 7, we present all the uncertainties on α computed in our analysis. Each point represents the mean of the corresponding upper and lower σ values. Besides the ideal cases of 1000 Patchy and LN mocks, we show the errors from CMASS jackknife and those from jackknife on 10 different Patchy and LN realizations. The errors are all consistent and we cannot identify a specific jackknife configuration that returns a better estimate of σ_α. The Patchy and LN mocks are different, but they converge in the 20 JK configuration.

It is noteworthy to mention that the alpha results in Fig. 7 include the Hartlap factor and demonstrate that this correction is needed for jackknife covariances. In fact, if we do not include it, the error on the 20 JK case would be smaller by $\sim \sqrt{0.42}$ (see Table 2). In conclusion, only when the Hartlap factor is applied all the jackknife configurations give a consistent error on α.

We have explored further the dependence of the α parameter and its uncertainty on the tapering parameter $T_{\rm p}$. In Fig. 8, we show the α results assuming $T_{\rm p} = [50, 100, 300, 500, 700]$. The top panel displays α from the 1000 LN mocks without jackknife and from jackknife applied to one of the LN; the bottom panel shows the CMASS jackknife outcomes. In the plots, we offset the tapering values by a multiplicative factor to avoid crowding (see caption of Fig. 8). The optimal value, which provides errors on α of $\sim$ 1–2 per cent, turns out to be $T_{\rm p} = 500$. In this way, our BOSS CMASS α estimates are comparable with previous results in the literature (pre-reconstruction, e.g. Ross et al. 2016; Pearson & Samushia 2018).

The 20 JK configuration shows the largest fluctuations due to the limited number of resamplings. We have further tested our MCMC code without including any tapering correction and leaving only the Hartlap factor. In this case, we find that the covariances from 20 JK resamplings are no longer semi-positive definite, meaning that they are not invertible, hence not useful for assembling the precision matrix needed to estimate α. Such a result confirms that jackknife configurations with few cells tend to provide non robust covariance estimates.

7 DISCUSSION AND SUMMARY

We have studied the impact of choosing different sizes and numbers of jackknife resamplings on the accuracy of the covariance estimates and the α shift parameter. To this purpose, we have measured the first two even multipoles of the BOSS CMASS DR12 galaxy sample at $0.43 < z < 0.7$ and we have modelled the results both using 1000 MultiDark Patchy mocks (Section 4.1), a set of 1000 lognormal mocks (Section 4.2) and an analytic approach (Section 4.3). We have computed their covariances using 200, 100, 50 and 20 jackknife resamplings coupled with two binning schemes: 20 or 10 linear bins in $24 < s < 184\,h^{-1}$Mpc, with 120 linear bins in $0 < \mu < 1$ (see Section 3). We have compared the results with the covariances obtained from the 1000 independent Patchy and LN mocks without jackknife. We have then applied the same jackknife configurations above on 10 different Patchy/LN realizations to derive covariances directly comparable with the CMASS ones.

From these different covariance matrices we have derived corresponding precision matrices (Section 5), which we have used as inputs for our Monte Carlo Markov Chain to estimate the baryon acoustic scale through the α shift parameter and its uncertainty. Our main findings are summarized in what follows:

(i) We find good consistency between the covariances obtained from CMASS, Patchy and LN jackknife resamplings, and from 1000 Patchy/LN without jackknife. This leads to consistent error bars in both the galaxy clustering measurements and the α shift parameter.

(ii) We find no evidence for a bias in the inferred value of α or its error when the jackknife cell size is smaller than the maximum 2PCF scale measured. However, with few resamplings available the error estimate becomes unreliable. This result may be due to the fact

Table 3. Estimates of the α shift parameter and its uncertainty obtained from the four jackknife configurations coupled with two binning schemes applied to the CMASS data, the lognormal lightcones and the Patchy mocks. For the LN and Patchy mocks, we show the mean α value obtained from the jackknife runs on 10 realizations randomly chosen. The last row shows the result obtained from the covariances of the 1000 LN or Patchy mocks without performing jackknife resampling. All these results here assume an optimal tapering parameter of $T_{\rm p} = 500$ and are shown in Fig. 6.

	α		
	BOSS CMASS	LN light-cones	PATCHY MOCKS
200 JK, 20 bins	$0.974^{+0.022}_{-0.020}$	$0.982^{+0.015}_{-0.014}$	$1.006^{+0.021}_{-0.025}$
100 JK, 20 bins	$0.978^{+0.017}_{-0.017}$	$0.975^{+0.011}_{-0.011}$	$0.990^{+0.023}_{-0.024}$
50 JK, 20 bins	$0.973^{+0.011}_{-0.011}$	$0.967^{+0.010}_{-0.010}$	$0.998^{+0.017}_{-0.019}$
20 JK, 10 bins	$0.980^{+0.019}_{-0.018}$	$0.990^{+0.017}_{-0.014}$	$0.989^{+0.018}_{-0.016}$
All LN (Patchy) w/o JK, 20 bins		$1.000^{+0.018}_{-0.017}$	$0.996^{+0.017}_{-0.016}$

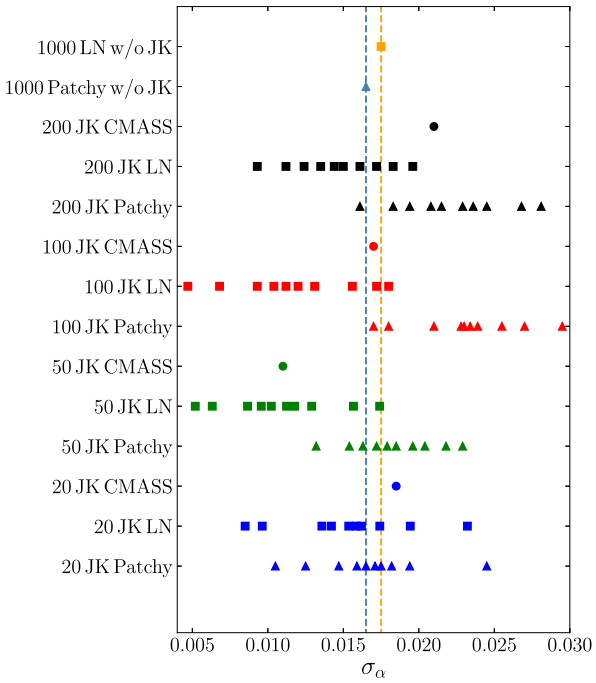

Figure 7. Uncertainties on the α shift parameter obtained from the 1000 Patchy and LN mocks without jackknife, and from the CMASS, 10 Patchy and 10 LN jackknife resamplings. The different sets of points are colour-coded as in Fig. 6 and the vertical lines help the comparison with the ideal cases of 1000 Patchy and LN mocks.

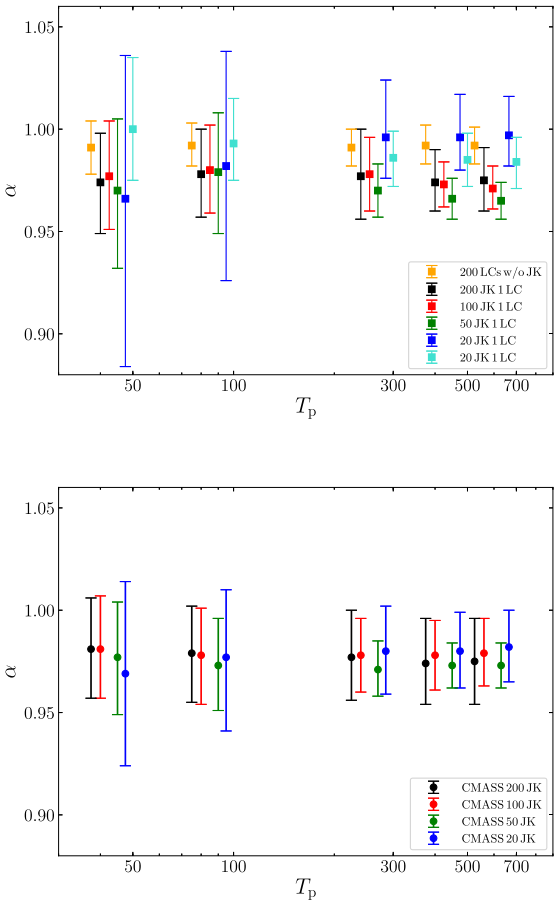

Figure 8. Shift parameter α and its uncertainty as a function of the tapering parameter $T_{\rm p}$. Top: Results from covariances computed from 200 LN mocks without jackknife and from jackknife performed on an LN realization. We have offset the $T_{\rm p}$ values on the x-axis by multiplying them, from left to right, by [0.75,0.80,0.85,0.90,0.95,1.0]. Bottom: results from CMASS jackknife resampling. The $T_{\rm p}$ values have been offset by multiplying them, from left to right, by [0.80,0.85,0.90,0.95,1.0].

that the JK volumes in our analysis have a dimension along the line of sight that is longer than the maximum pair separation. Thus, even though we find no effect on the isotropic α parameter, there may be a bias if we separate the LOS and transverse modes by fitting $\alpha_{\rm \shortparallel}$ and $\alpha_{\perp}$.

(iii) We have demonstrated that it is useful to apply the Hartlap factor and the tapering scheme to estimate the precision matrix with jackknife resampling. The α shift parameter estimated either from CMASS, Patchy or LN jackknife covariances, or from 1000 independent Patchy or LN mocks without jackknife, are all consistent between each other and in reasonable agreement with previous BOSS CMASS DR12 results from galaxy clustering pre-reconstruction analysis (Ross et al. 2016). We find uncertainties on α of 1-2.5 per cent, depending on the jackknife size and 2PCF binning scheme adopted. This confirms that the jackknife methodology applied to both observations and mocks produces a comparable level of noise in the covariance estimates. This noise is then reduced in the precision matrix by applying the tapering correction (see Section 5).

(iv) We have tested different values for the tapering parameter, in the range $50 \leq T_{\rm p} \leq 700$, to maximize the accuracy in the α shift parameter estimation. We find that the optimal value is $T_{\rm p} = 500$. By

lowering it, the noise in the precision matrix estimate is suppressed but the error on α grows.

To summarize, performing jackknife resamplings either on BOSS CMASS DR12 data, Patchy or lognormal mocks with the same CMASS volume provides covariances that are consistent with those obtained from a set of 1000 independent Patchy or LN mocks and with previous results in the literature (Ross et al. 2016). These covariances lead to α estimates with 1–2.5 per cent uncertainties, depending on the jackknife size/2PCF binning scheme assumed.

The largest differences between covariance estimates from jackknife resampling and 1000 independent mock realizations without JK are visible in the off-diagonal terms. Here, the jackknife results exhibit a higher level of noise. This difference is key for determining the accuracy of the α shift parameter. The action of the tapering correction (Section 5) is to considerably reduce this noise returning comparable uncertainties on α from all of the different covariance estimates tested.

Although previous works limit the jackknife scale to larger than the measured 2PCF scale (e.g. Beutler et al. 2011; Hong et al. 2016), we find that this is not essential. In fact, when using jackknife to estimate covariances, one should prioritize building a large number of resamplings rather than choosing a jackknife size larger than the maximum galaxy clustering scale measured. In fact, especially when studying BAO scales, by requiring $S_{\rm JK} \geq \max(s)$, we are able to build only few wide jackknife regions, which leads to large uncertainties in the error estimates. In our results, we do not see a clear trend that the α error bars tend to reduce with a specific jackknife configuration. All the JK configurations tested return consistent errors.

The new generation of cosmological surveys, such as DESI, Euclid or LSST, will span larger volumes compared to SDSS-III/BOSS. The precision in their covariance estimates based on thousands of independent mock realizations will depend on the feasibility (and our ability) of producing large synthetic data sets. Whenever mocks will not be available, the jackknife method can be used to obtain reasonable covariance estimates. The precision of the cosmological parameters inferred from the jackknife covariances will be determined in part by the number of resamplings.

We find that it is not essential to use jackknife sizes larger than the BAO scale, and so it will be possible to achieve $N > 10^3$ resamplings to reach per cent level precision on the error of cosmological parameters using the jackknife approach. From our analysis we have found that the covariance estimates are less noisy when a large number of jackknife resamplings is performed. However, the noise in the covariances has relatively small effect on the α uncertainty. In a follow-up work, we will address the feasibility of inferring covariance estimates for a survey such as Euclid using a large number of jackknife resamplings.

ACKNOWLEDGEMENTS

GF acknowledges financial support from the SNF 175751 'Cosmology with 3D Maps of the Universe' research grant.

GF thanks the Institute of Cosmology and Gravitation at Portsmouth University to host and fund her through a Dennis Sciama fellowship during the first part of this project.

DS acknowledges financial support from the Fondecyt Regular project number 1200171.

The authors are thankful to Cheng Zhao, who provided the 1000 Patchy pair counts, allowing them to save a considerable amount of time.

Funding for SDSS-III has been provided by the Alfred P. Sloan Foundation, the Participating Institutions, the National Science Foundation, and the U.S. Department of Energy Office of Science. The SDSS-III web site is http://www.sdss3.org/.

SDSS-III is managed by the Astrophysical Research Consortium for the Participating Institutions of the SDSS-III Collaboration including the University of Arizona, the Brazilian Participation Group, Brookhaven National Laboratory, Carnegie Mellon University, University of Florida, the French Participation Group, the German Participation Group, Harvard University, the Instituto de Astrofisica de Canarias, the Michigan State/Notre Dame/JINA Participation Group, Johns Hopkins University, Lawrence Berkeley National Laboratory, Max Planck Institute for Astrophysics, Max Planck Institute for Extraterrestrial Physics, New Mexico State University, New York University, Ohio State University, Pennsylvania State University, University of Portsmouth, Princeton University, the Spanish Participation Group, University of Tokyo, University of Utah, Vanderbilt University, University of Virginia, University of Washington, and Yale University.

DATA AVAILABILITY

The BOSS DR12 CMASS data analysed in this work are publicly available at https://dr12.sdss.org/sas/dr12/boss/lss/, The 1000 Patchy mocks can be downloaded at https://data.sdss.org/sas/dr12/boss/lss/dr12_multidark_patchy_mocks/. The 1000 lognormal mocks have been generated using *Synmock* and they are available upon request to the authors.

REFERENCES

Ade P. A. R. et al., 2016, Astron. Astrophys., 594, A13
Agrawal A., Makiya R., Chiang C.-T., Jeong D., Saito S., Komatsu E., 2017, J. Cosmol. Astropart. Phys., 2017, 003
Ahn C. P. et al., 2012, ApJS, 203, 21
Aihara H. et al., 2011, ApJS, 193, 29
Alam S. et al., 2015, ApJS, 219, 12
Alam S. et al., 2017, MNRAS, 470, 2617
Ali-Haïmoud Y., Bird S., 2013, MNRAS, 428, 3375
Anderson L. et al., 2012, MNRAS, 427, 3435
Avila S., Murray S. G., Knebe A., Power C., Robotham A. S. G., Garcia-Bellido J., 2015, MNRAS, 450, 1856
Baugh C. M., 2006, Rep. Progr. Phys., 69, 3101
Benson A. J., 2010, Phys. Rep., 495, 33
Benson A. J., 2012, 17, 175
Berlind A. A., Weinberg D. H., 2002, ApJ, 575, 587
Bernardeau F., 1994, ApJ, 427, 51
Beutler F. et al., 2011, MNRAS, 416, 3017
Blas D., Lesgourgues J., Tram T., 2011, J. Cosmol. Astropart. Phys., 2011, 034
Blot L. et al., 2019, MNRAS, 485, 2806
Bolton A. S. et al., 2012, AJ, 144, 144
Bouchet F. R., Colombi S., Hivon E., Juszkiewicz R., 1995, A&A, 296, 575
Bower R. G., Benson A. J., Malbon R., Helly J. C., Frenk C. S., Baugh C. M., Cole S., Lacey C. G., 2006, MNRAS, 370, 645
Buchert T., 1994, MNRAS, 267, 811
Catelan P., Lucchin F., Matarrese S., Moscardini L., 1995, MNRAS, 276, 39
Chuang C.-H. et al., 2015b, MNRAS, 452, 686
Chuang C.-H., Kitaura F.-S., Prada F., Zhao C., Yepes G., 2015a, MNRAS, 446, 2621
Coles P., Jones B., 1991, MNRAS, 248, 1
Collacchioni F., Cora S. A., Lagos C. D. P., Vega-Martínez C. A., 2018, MNRAS, 481, 954
Cora S. A. et al., 2018, MNRAS, 479, 2
Cora S. A., 2006, MNRAS, 368, 1540

Crain R. A. et al., 2015, MNRAS, 450, 1937
Crocce M., Scoccimarro R., 2006, Phys. Rev., D73, 063519
Croton D. J. et al., 2006, MNRAS, 365, 11
Croton D. J. et al., 2016, ApJS, 222, 22
Davison A. C., Hinkley D. V., 1997, Bootstrap Methods and Their Application. Cambridge Univ. Press, Cambridge, p. i
De Lucia G., Boylan-Kolchin M., Benson A. J., Fontanot F., Monaco P., 2010, MNRAS, 406, 1533
Efron B., 1979, Ann. Statist., 7, 1
Eisenstein D. J. et al., 2005, ApJ, 633, 560
Eisenstein D. J., Hu W., 1998, ApJ, 496, 605
Favole G., McBride C. K., Eisenstein D. J., Prada F., Swanson M. E., Chuang C.-H., Schneider D. P., 2016a, MNRAS, 462, 2218
Favole G., McBride C. K., Eisenstein D. J., Prada F., Swanson M. E., Chuang C.-H., Schneider D. P., 2016b, MNRAS, 462, 2218
Favole G., Rodríguez-Torres S. A., Comparat J., Prada F., Guo H., Klypin A., Montero-Dorta A. D., 2017, MNRAS, 472, 550
Favole G., Sapone D., Silva Lafaurie J., 2019, preprint (arXiv:1912.06155)
Feldman H. A., Kaiser N., Peacock J. A., 1994, ApJ, 426, 23
Feng Y., Chu M.-Y., Seljak U., McDonald P., 2016, MNRAS, 463, 2273
Font A. S., Johnston K. V., Ferguson A. M. N., Bullock J. S., Robertson B. E., Tumlinson J., Guhathakurta P., 2008, ApJ, 673, 215
Fukugita M., Ichikawa T., Gunn J. E., Doi M., Shimasaku K., Schneider D. P., 1996, AJ, 111, 1748
Gargiulo I. D. et al., 2015, MNRAS, 446, 3820
Genel S. et al., 2014, MNRAS, 445, 175
Gonzalez-Perez V., Lacey C. G., Baugh C. M., Lagos C. D. P., Helly J., Campbell D. J. R., Mitchell P. D., 2014, MNRAS, 439, 264
Górski K. M., Hivon E., Banday A. J., Wand elt B. D., Hansen F. K., Reinecke M., Bartelmann M., 2005, ApJ, 622, 759
Gunn J. E. et al., 1998, AJ, 116, 3040
Gunn J. E. et al., 2006, AJ, 131, 2332
Guo Q. et al., 2011, MNRAS, 413, 101
Guo H. et al., 2013, ApJ, 767, 122
Guo H. et al., 2015a, MNRAS, 449, L95
Guo H. et al., 2015b, MNRAS, 453, 4368
Hartlap J., Simon P., Schneider P., 2007, A&A, 464, 399
Henriques B., Maraston C., Monaco P., Fontanot F., Menci N., De Lucia G., Tonini C., 2011, MNRAS, 415, 3571
Henriques B. M. B., White S. D. M., Thomas P. A., Angulo R. E., Guo Q., Lemson G., Springel V., 2013, MNRAS, 431, 3373
Hirschmann M., De Lucia G., Fontanot F., 2016, MNRAS, 461, 1760
Hong T., Han J. L., Wen Z. L., 2016, ApJ, 826, 154
Hou J., Lacey C. G., Frenk C. S., 2018, MNRAS, 475, 543
Howlett C., Manera M., Percival W. J., 2015, Astron. Comput., 12, 109
Hu W., Sugiyama N., 1996, ApJ, 471, 542
Ivezić Ž. et al., 2019, ApJ, 873, 111
Izard A., Crocce M., Fosalba P., 2016, MNRAS, 459, 2327
Kauffmann G., White S. D. M., Guiderdoni B., 1993, MNRAS, 264, 201
Kaufman C. G., Schervish M. J., Nychka D. W., 2008, J. Am. Stat. Assoc., 103, 1545
Kitaura F. S., Hess S., 2013, MNRAS, 435, L78
Kitaura F. S., Yepes G., Prada F., 2014, MNRAS, 439, L21
Kitaura F.-S. et al., 2016, MNRAS, 456, 4156
Kitaura F.-S., Gil-Marín H., Scóccola C. G., Chuang C.-H., Müller V., Yepes G., Prada F., 2015, MNRAS, 450, 1836
Klypin A., Prada F., 2018, MNRAS, 478, 4602
Koda J., Blake C., Beutler F., Kazin E., Marin F., 2016, MNRAS, 459, 2118
Lagos C. d. P., Lacey C. G., Baugh C. M., 2013, MNRAS, 436, 1787
Lagos C. D. P., Baugh C. M., Lacey C. G., Benson A. J., Kim H.-S., Power C., 2011, MNRAS, 418, 1649
Landy S. D., Szalay A. S., 1993, ApJ, 412, 64
Laureijs R. et al., 2011, preprint (arXiv:1110.3193)
Lesgourgues J., 2011 preprint (arXiv:1104.2932)
Lippich M. et al., 2019, MNRAS, 482, 1786
Manera M. et al., 2013, MNRAS, 428, 1036
Miller R. G., 1974, Biometrika, 61, 1
Mo H., van den Bosch F. C., White S., 2010, Galaxy Formation and Evolution
Mohayaee R., Mathis H., Colombi S., Silk J., 2006, MNRAS, 365, 939
Monaco P., Theuns T., Taffoni G., 2002, MNRAS, 331, 587
Monaco P., Sefusatti E., Borgani S., Crocce M., Fosalba P., Sheth R. K., Theuns T., 2013, MNRAS, 433, 2389
Monaco P., Benson A. J., De Lucia G., Fontanot F., Borgani S., Boylan-Kolchin M., 2014, MNRAS, 441, 2058
Naab T., Ostriker J. P., 2017, Ann. Rev. Astron. Astrophys., 55, 59
Neyrinck M. C., 2013, MNRAS, 428, 141
Norberg P., Baugh C. M., Gaztañaga E., Croton D. J., 2009, MNRAS, 396, 19
Norberg P., Gaztañaga E., Baugh C. M., Croton D. J., 2011, MNRAS, 418, 2435
Padmanabhan N., White M. J., 2008, Phys. Rev., D77, 123540
Parimbelli G., Viel M., Sefusatti E., 2019, J. Cosmol. Astropart. Phys., 2019, 010
Paz D. J., Sánchez A. G., 2015, MNRAS, 454, 4326
Pearson D. W., Samushia L., 2018, MNRAS, 478, 4500
Pearson D. W., Samushia L., Gagrani P., 2016, MNRAS, 463, 2708
Pillepich A. et al., 2018, MNRAS, 473, 4077
Planck et al., 2014, A&A, 571, A16
Quenouille M. H., 1956, Biometrika, 43, 353
Reid B. et al., 2016, MNRAS, 455, 1553
Rodríguez-Torres S. A. et al., 2016, MNRAS, 460, 1173
Ross A. J. et al., 2012, MNRAS, 424, 564
Ross A. J. et al., 2016, MNRAS, 464, 1168
Sánchez A. G. et al., 2012, MNRAS, 425, 415
Sartoris B. et al., 2016, MNRAS, 459, 1764
Schaye J. et al., 2015, MNRAS, 446, 521
Schlegel D. J. et al., 2015, American Astronomical Society Meeting Abstracts #225. p. 336.07
Scoccimarro R., Sheth R. K., 2002, MNRAS, 329, 629
Smee S. A. et al., 2013, AJ, 146, 32
Somerville R. S., Davé R., 2015, ARA&A, 53, 51
Springel V., 2010, MNRAS, 401, 791
Springel V., Hernquist L., 2003, MNRAS, 339, 312
Stevens A. R. H., Brown T., 2017, MNRAS, 471, 447
Takahashi R., Sato M., Nishimichi T., Taruya A., Oguri M., 2012, ApJ, 761, 152
Tassev S., Zaldarriaga M., Eisenstein D. J., 2013, J. Cosmol. Astropart. Phys., 2013, 036
Tonini C., Maraston C., Devriendt J., Thomas D., Silk J., 2009, MNRAS, 396, L36
Turkey J., 1958, Ann. Math. Stat., 29, 1
Vogelsberger M. et al., 2014a, MNRAS, 444, 1518
Vogelsberger M. et al., 2014b, Nature, 509, 177
Weinmann S. M., van den Bosch F. C., Yang X., Mo H. J., 2006, MNRAS, 366, 2
White S. D. M., Frenk C. S., 1991, ApJ, 379, 52
White M., Tinker J. L., McBride C. K., 2014, MNRAS, 437, 2594
Wright B. S., Winther H. A., Koyama K., 2017, J. Cosmol. Astropart. Phys., 2017, 054
Xu X., Padmanabhan N., Eisenstein D. J., Mehta K. T., Cuesta A. J., 2012, MNRAS, 427, 2146
Yepes G., Kates R., Khokhlov A., Klypin A., 1997, MNRAS, 284, 235
Yoshida N., Sokasian A., Hernquist L., Springel V., 2003, ApJ, 598, 73
Zehavi I. et al., 2002, ApJ, 571, 172
Zehavi I. et al., 2005, ApJ, 630, 1
Zehavi I. et al., 2011, ApJ, 736, 59
Zheng Z. et al., 2005, ApJ, 633, 791

This paper has been typeset from a TEX/LATEX file prepared by the author.